Engineering Fracture Mechanics 78 (2011) 2775–2788

Contents lists available at SciVerse ScienceDirect

Engineering Fracture Mechanics

journal homepage: www.elsevier.com/locate/engfracmech

Examination of the Mode II fracture behaviour of wood with a short crack in an asymmetric four-point bending test

Cicilia Maria Erna Susanti, Tetsuya Nakao, Hiroshi Yoshihara *

Faculty of Science and Engineering, Shimane University, Nishikawazu-cho 1060, Matsue, Shimane 690-8504, Japan

ARTICLE INFO

Article history:
Received 1 October 2010
Received in revised form 9 July 2011
Accepted 29 July 2011

Keywords:
Asymmetric four-point bending test
Mode II stress intensity factor
Shear strength
Correction crack length
Short crack

ABSTRACT

Asymmetric four-point bending tests of agathis specimens with a short crack along the neutral axis in a tangential–longitudinal system were conducted onto analyse the failure behaviour of wood with a short crack. The nominal shear strength and Mode II critical stress intensity factors of the specimens with various crack lengths were measured, and the influence of crack length on these properties was examined. The nominal shear strength of the cracked specimens was significantly lower than the strength of a crack-free specimen, even when the crack was extremely short. This finding suggests that the fracture mechanics theory is effective for analysing the failure behaviour of wood with a very short crack in this loading condition. However, the Mode II critical stress intensity factor still depends on the crack length. When the crack length was corrected with considering the formation of fracture process zone ahead of the crack tip, the critical intensity factor could be predicted effectively as well as the nominal shear strength.

1. Introduction

Over the years, the failure and fracture behaviours of materials with short cracks have been analysed in studies on various metals. According to the research on aluminium 7076-T6 by Irwin et al. [1], the nominal strength value of a cracked specimen coincides approximately with the actual strength of the specimen, which is measured using a crack-free specimen when the crack is shorter than a certain critical length. Therefore, the fracture mechanics theory is not effective for predicting the failure behaviour of specimens with a short crack. This phenomenon was described in many texts on fracture mechanics and it is reasonable to assume that this theory could be widely applicable to various materials including wood [2]. Nevertheless, the bending failure and Mode I fracture behaviours of wood with short cracks are extremely contradictory based on descriptions in the current texts. In previous studies, single-edge-notched bending (SENB) tests of agathis were conducted using specimens with a short crack, and it was suggested that the Mode I critical stress intensity factor could be predicted effectively when the crack length was corrected [3,4]. The correction of crack length also enables the prediction of nominal bending strength of cracked and crack-free specimens based on fracture mechanics theory. These behaviours may also be applicable for those obtained from the other conditions, such as shear-dominant condition in which in-plane shear failure or Mode II fracture propagation is induced.

To examine the in-plane shear failure and Mode II fracture behaviours of materials with short cracks, Mode II fracture tests should be conducted using cracked and crack-free specimens. End-notched flexure (ENF) tests are usually conducted because the Mode II energy release rate G_{II} can be determined in a rigorous manner [5–9]. Nevertheless, it is difficult to conduct ENF tests using specimens with short cracks. This difficulty is also applicable to other Mode II fracture test methods,

* Corresponding author. Tel.: +81 852 32 6508; fax: +81 852 32 6123.
E-mail address: yosihara@riko.shimane-u.ac.jp (H. Yoshihara).

0013-7944/$ - see front matter © 2011 Elsevier Ltd. All rights reserved.
doi:10.1016/j.engfracmech.2011.07.014

Nomenclature

$2a$	crack length
$2a_0$	initial crack length
$2a_{eq}$	equivalent crack length
C	loading-line compliance
C_0	initial loading-line compliance
C_c	loading-line compliance at the initiation of crack propagation
E_L	Young's modulus in the longitudinal direction
E_R	Young's modulus in the radial direction
E_T	Young's modulus in the tangential direction
$f(2a/s)$	crack geometry factor
F_x^j	nodal force at the crack tip in the x-direction
F_y^j	nodal force at the crack tip in the y-direction
F_z^j	nodal force at the crack tip in the z-direction
G	energy release rate
G_{II}	Mode II energy release rate
G_{LR}	shear modulus in the longitudinal–radial plane
G_{LT}	shear modulus in the longitudinal–tangential plane
G_{RT}	shear modulus in the radial–tangential plane
K	stress intensity factor
K_{II}	Mode II stress intensity factor
K_{IIc}	critical value of the Mode II stress intensity factor
P	applied load
P_c	critical load for crack propagation
s	shear span
T	thickness at the middle section of the specimen
v	loading-line displacement
W	depth of the specimen
x	vertical direction of the specimen
y	horizontal direction of the specimen
δ_x^i	relative crack face displacement between the nodes adjacent to the crack tip in the x-direction
δ_y^i	relative crack face displacement between the nodes adjacent to the crack tip in the y-direction
δ_z^i	relative crack face displacement between the nodes adjacent to the crack tip in the z-direction
Δ	additional crack length
Δ_x	length in the x-direction of the element at the delamination front
Δ_y	length in the y-direction of the element at the delamination front
Δ_z	length in the z-direction of the element at the delamination front
ν_{LR}	Poisson's ratio in the longitudinal–radial plane
ν_{LT}	Poisson's ratio in the longitudinal–tangential plane
ν_{RT}	Poisson's ratio in the radial–tangential plane
τ_n	nominal shear stress
τ_{nc}	nominal shear strength

List of acronyms

3ENF	three-point bend end-notched flexure
AFPB	asymmetric four-point bending
ENF	end-notched flexure
FPZ	fracture process zone
VCCT	virtual crack closure technique

such as compact shear (CS) [10], double edge notched shear (DENS) [10,11]. In addition, it is difficult to obtain the actual shear strength of crack-free specimen from the CS and DENS tests. In contrast, asymmetric four-point bending (AFPB) tests using tapered specimens (details of the specimens are described below) enabled the examination of the in-plane shear failure and Mode II fracture behaviours of wood with a short crack.

In the present study, AFPB tests were performed with specimens of agathis with varying crack lengths that were much shorter than the lengths that were utilised in several existing studies involving ENF tests [5–9]. The nominal shear strength and Mode II critical stress intensity factor were analysed based on elementary beam theory and linear fracture mechanics

theory, respectively. The results ultimately revealed the appropriate method for analysing the failure and fracture behaviours of wood with short cracks.

2. Asymmetric four-point bending test analyses for a cracked specimen

Fig. 1 shows a schematic diagram of the asymmetric four-point bending (AFPB) test for a tapered specimen with a short crack along the neutral axis. Murphy conducted the AFPB test on wood from a Douglas fir with a straight specimen with a long crack to measure the Mode II critical stress intensity factor [12]. When the crack was short or does not exist, however, failure by bending behind the loading point cannot be prevented [13]. Therefore, the cutting of tapers on both sides of the specimen was therefore effective for preventing the specimen from failure through bending [14]. A specimen with a crack of length $2a$ at its centre was asymmetrically supported at two trisected points and the loads were applied at the remaining two points. The crack length was defined as $2a$, and the distance between the supporting and loading points, which is called shear span, was defined as s. Under these loading conditions, the nominal shear stress along the neutral axis of the middle section τ_n was derived from elementary beam theory as follows [14]:

$$\tau_n = \frac{3P}{4WT}, \tag{1}$$

where W is the beam depth, T is the thickness at the middle section, and P is the applied load. This notation is also applicable to crack-free specimens. When a crack-free specimen was bent, the failure-by-shearing force was induced at the neutral axis when τ_n reached its critical value τ_{nc}, which was defined as the shear strength of the material.

Fracture behaviour is generally analysed with the stress intensity factor K or the energy release rate G. Each factor is derived from fracture mechanics theory. The value of G can be determined with energy considerations and is mathematically well defined, while K is regarded as a localised parameter that is influenced by microstructural, local anisotropy [15]. In terms of rigor, the measurement of G, which requires the load–deformation relation to correspond to the crack length, is preferable to the rigor of K. For measuring the Mode II energy release rate G_{II} by an AFPB test, a compliance calibration method, which requires the relationship between the loading-line compliance and crack length, can be adopted. Nevertheless, it is difficult to detect the variation of compliance because of the small crack length variation. In contrast, the Mode II stress intensity factor K_{II}, which does not require the loading-line compliance, is more easily measured with an approximating equation and is less mathematically rigorous.

The Mode II stress intensity factor K_{II} was derived using the following equation:

$$K_{II} = \tau_n \sqrt{\pi a} f\left(\frac{2a}{s}\right), \tag{2}$$

where $f(2a/s)$ is the crack geometry factor, which is usually determined by finite element method (FEM) calculations. The fracture was initiated when K_{II} reached the critical stress intensity factor, defined as K_{IIc}, which was obtained by substituting τ_{nc} for τ_n in Eq. (2).

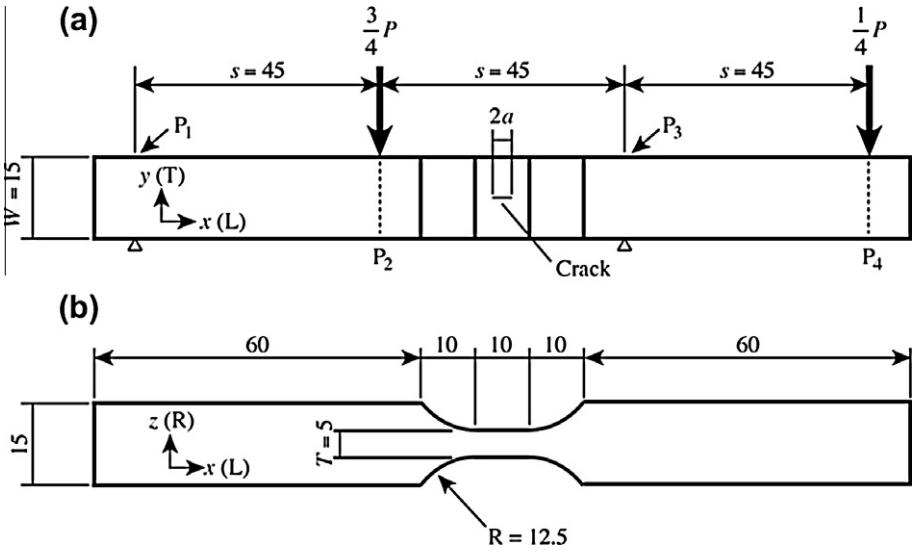

Fig. 1. Schematic diagram of the asymmetric four-point bending (AFPB) test of a notched specimen. (a) Side view, (b) top view. Unit = mm. L, T, and R represent the longitudinal, tangential, and radial directions, respectively.

3. Finite element calculations

To determine the crack geometry factor $f(2a/s)$, three-dimensional FEM calculations were performed using ANSYS version 5.7 from the Information Initiative Center of Hokkaido University. Fig. 2 shows the finite element mesh of the AFPB specimen. The crack length $2a$ varied from 1 to 8 mm at intervals of 1 mm. The mesh was refined closer to the crack tip, as shown in Fig. 2c and d. Table 1 shows the elastic properties used in the calculations. These properties were determined by the compression and vibration tests described in Section 4.2. The length, thickness, and width directions of the model were defined as the x-, y-, and z-directions, respectively. These directions corresponded to the longitudinal (L), tangential (T), and radial (R) directions of the wood. A crack was produced along the L direction in the LT plane, which is the so-called TL system.

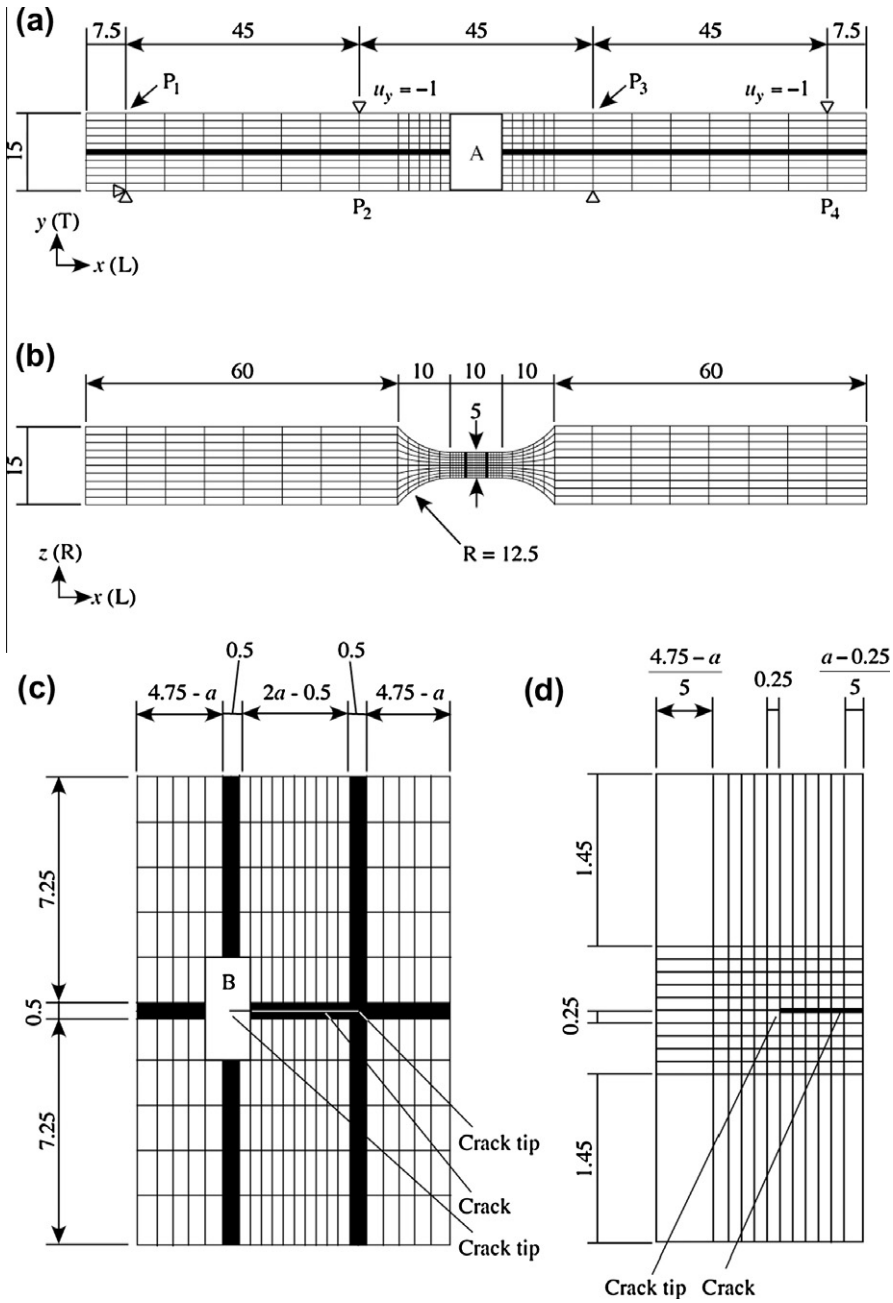

Fig. 2. The finite element model used for the AFPB test analysis. Unit = mm. L, T, and R represent the longitudinal, tangential, and radial directions, respectively. (a) Top view of the overall mesh, (b) side view of the overall mesh, (c) details of Zone A in (a) and (d) details of Zone B in (c). The crack length $2a$ varied from 1 to 8 mm at intervals of 1 mm.

Table 1
Elastic constants used for the finite element calculation.

Young's modulus (GPa)			Shear modulus (GPa)			Poisson's ratio		
E_L	E_T	E_R	G_{LT}	G_{TR}	G_{LR}	ν_{LT}	ν_{TR}	ν_{LR}
14.6	0.68	0.87	0.84	0.14	1.00	0.44	0.45	0.44

L, R, and T represent the longitudinal, radial, and tangential directions, respectively.

The models were asymmetrically supported in the vertical direction at x = 7.5 mm and at x = 97.5 mm. Additionally, a vertical displacement u_y of 1 mm was asymmetrically applied downward at the node at x = 52.5 mm and at x = 142.5 mm.

Mode I, Mode II, and Mode III strain energy release rate components were calculated with the three-dimensional virtual crack closure technique (VCCT) [16] as follows:

$$\begin{cases} G_{\mathrm{I}} = \frac{F_y^j \delta_y^i}{2\Delta_x \Delta_z} \\ G_{\mathrm{II}} = \frac{F_x^j \delta_x^i}{2\Delta_x \Delta_z} \\ G_{\mathrm{III}} = \frac{F_z^j \delta_z^i}{2\Delta_x \Delta_z} \end{cases}, \tag{3}$$

where F_x^j, F_y^j, and F_z^j are the nodal forces at the crack tip node j in the x-, y-, and z-directions, respectively, Δ_x and Δ_z are the lengths in the x- and z-direction of the element at the crack tip. Additionally, δ_x^i, δ_y^i, and δ_z^i are the relative displacements between nodes i and i', which are located at a distance Δ_x (=0.25 mm) behind the crack tip in the x-, y-, and z-directions, respectively. In the calculations, the Mode I and Mode III strain energy release rate components were almost zero. As such, the fracture mechanics behaviour could be considered a part of the pure Mode II condition.

In addition to the VCCT, the value of G_{II} was calculated from the relationship between the loading-line compliance C and half crack length a based on the compliance calibration method. To reduce the influence of indentation at the loading and supporting points, the displacements at the points P_1, P_2, P_3, and P_4 in Fig. 2, which were defined as v_1, v_2, v_3, and v_4, respectively, were obtained. The loading-line displacement v was obtained by the following equation:

$$v = \frac{1}{2}(v_2 + v_4) - \frac{1}{2}(v_1 + v_3), \tag{4}$$

The loading-line compliance C was derived as v/P, and the C–a relationship was obtained by varying a. The relationship was approximated by the following 4th polynomial equation:

$$C = A_0 + A_1 a + A_2 a^2 + A_3 a^3 + A_4 a^4, \tag{5}$$

The strain energy release rate obtained by this model should be halved because this model contains two crack tips, so it is calculated from the work required to let one equivalent crack tip propagate. Using Eq. (5), the value of G_{II} was given as:

$$G_{\mathrm{II}} = \frac{1}{2} \cdot \frac{P^2}{2B} \cdot \frac{\partial C}{\partial a} = \frac{P^2}{4B}\left(A_1 + 2A_2 a + 3A_3 a^2 + 4A_4 a^3\right), \tag{6}$$

The value of G_{II} obtained by the VCCT was transformed into the Mode II stress intensity factor K_{II} by the following equations [17]:

$$K_{\mathrm{II}} = \sqrt{\frac{E_x G_{\mathrm{II}}}{c_{\mathrm{II}}}}, \tag{7}$$

where E_x is Young's modulus in the x-direction, which corresponds to the L direction, and

$$c_{\mathrm{II}} = \frac{1}{\sqrt{2}} \sqrt{\sqrt{\frac{E_x}{E_y}} + \frac{1}{2}\left(\frac{E_x}{G_{xy}} - 2\nu_{xy}\right)}, \tag{8}$$

where E_y is Young's modulus in the y-direction, which corresponds to the T direction, and G_{xy} and ν_{xy} are the shear modulus and Poisson's ratio in the xy-plane, which corresponds to the LT plane, respectively. The crack geometry factor $f(2a/s)$ was derived from Eqs. (1), (2), and (7) as follows:

$$f\left(\frac{2a}{s}\right) = \frac{4WT}{3P\sqrt{\pi a}} \sqrt{\frac{E_x G_{\mathrm{II}}}{c_{\mathrm{II}}}}. \tag{9}$$

By substituting the total load applied to the finite element model P and G_{II} as calculated by the VCCT into this equation, a value of $f(2a/s)$ corresponding to the crack length-to-shear span ratio $2a/s$ was obtained.

4. Experiment

4.1. Materials

Agathis (*Agathis* sp.) lumber, with a density of 480 ± 10 kg/m^3 with 12% moisture content (MC) was used for the tests. The lumber had no defects such as knots or grain distortions so that the specimens cut from it could be regarded as small and clear. The lumber was stored for several months in a room at a constant temperature of 20 °C and a relative humidity of 65% before the test. The wood was confirmed to be in an air-dried condition. These conditions were maintained throughout the tests. The equilibrium MC was approximately 12%.

4.2. Compression and vibration tests for measuring the elastic constants

For the FEM analyses, Young's moduli in the L, T, and R directions (E_L, E_T, and E_R, respectively), the shear moduli in the LT, TR, and LR planes, (G_{LT}, G_{TR}, and G_{LR}, respectively), and Poisson's ratio in the LT, TR, and LR planes, (n_{LT}, n_{TR}, and n_{LR}, respectively), were required. These constants were measured through compression and vibration tests.

The Young's moduli and Poisson's ratios were measured by compression tests. A short-column specimen with dimensions of 30 mm × 15 mm × 15 mm was prepared from the lumber described above. The long axis coincided with the direction where Young's modulus was to be measured. Biaxial-strain gauges (gauge length = 2 mm; FCA-2-11, Tokyo Sokki Kenkyujo Co., Ltd., Tokyo, Japan) were bonded at the centres of the planes where the Young's moduli and Poisson's ratios were to be measured, and a compression load was applied along the long axis of the specimen at a crosshead speed of 0.5 mm/min. From the stress–strain relationship in the loading direction, Young's moduli were obtained. Poisson's ratios were obtained from the relationship between the loading and transverse strains.

The shear moduli were determined by free–free flexural vibration tests. A beam specimen with dimensions of 140, 30, and 15 mm in length, thickness, and width, respectively, was prepared. The specimen was suspended by threads at the nodal positions of the free–free resonance vibration mode and the specimen was excited in the width direction by a hammer. The first to fourth resonance frequencies in bending were measured and analysed by a fast Fourier transform (FFT) analysis program. The shear modulus in the length–thickness plane was calculated by Hearmon's iteration method, the details of which are described in [18].

4.3. Asymmetric four-point bending tests of cracked and crack-free specimens

All of the specimens were cut from the lumber described above so that they were long-matched. The specimens initially had the dimensions of 150 (L) × 15 (T) × 15 (R) mm^3. As shown in Fig. 1b, tapers were cut on both LT planes by a router. The width at the middle section was 5 mm.

For cracked specimens, the crack was produced along the L direction in the TL system. In this experiment, it was difficult to use a band saw and razor blade, which was used in several previous investigations [5–12] since the crack was too short to use these tools. Instead, multiple holes (diameter = 0.5 mm) were first cut with a drill. Then the holes were connected with each other with an electrodeposited wire (diameter = 0.265 mm). The crack was finally extended to the length as described below with the wire. There was a concern that the crack tip cut by the wire was blunt. In the preliminary tests, AFPB tests were conducted using the specimens with a long crack, which was extended by the wire and razor blade. It was confirmed that the sharpness of the crack tip cut by the wire was similar to the tip cut by the razor blade. The crack length $2a$ varied from 0 (crack-free specimen) to 8 mm by intervals of 2 mm. Five specimens were used for each test condition.

Fig. 3 shows the experimental setup of the AFPB test. Each specimen was supported asymmetrically at two trisected points and loaded at the remaining two trisected points. The radius of loading and supporting nose was 15 mm. Then a load was applied to the specimen at a crosshead speed of 1 mm/min. The test was conducted until the load markedly decreased. As shown in this figure, the displacements at the points behind the loading and supporting points were measured by four cantilever type displacement transducers (CE-10, Tokyo Sokki Kenkyujo Co., Ltd., Tokyo, Japan). The loading-line displacement v was calculated using Eq. (4).

Fig. 4 shows a typical relationship between the load and loading-line displacement obtained by the AFPB test. The load initially increases linearly, then it increases nonlinearly until it reaches the maximum value, then it drops immediately.

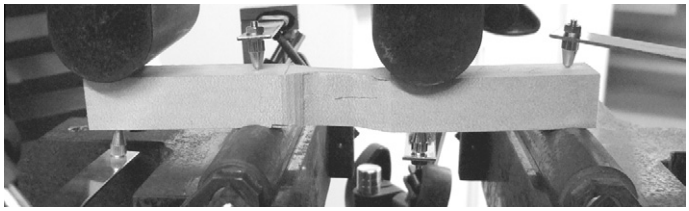

Fig. 3. Experimental setup of the AFPB test.

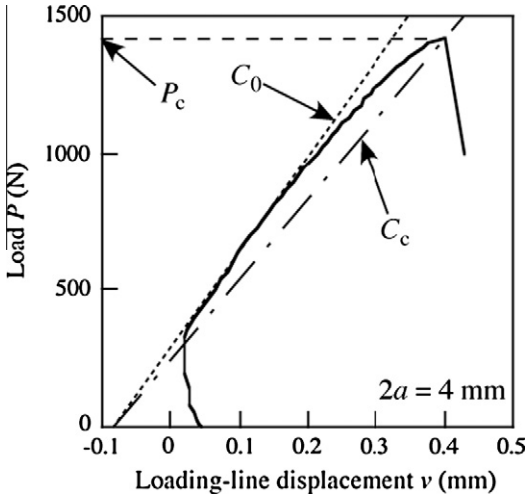

Fig. 4. Typical example of the relationship between the load P and loading-line displacement v. C_0, C_c, and P_c represent the initial loading-line compliance, loading-line compliance at the initiation of crack propagation, and the critical load for crack propagation, respectively.

Based on our observations of the test, the crack propagation occurred when the load was close to its peak value. As noted in previous studies [19,20], loading-line compliance increases before the load reaches its maximum value because the fracture process zone (FPZ), a region of low stiffness, is produced ahead of the crack tip. Because of the FPZ, the effective crack length does not correspond to the initial crack length at peak load. Additionally, Dourado et al. pointed out that the real crack initiation occurred markedly after the peak load [21]. Although stable crack propagation was not observed during loading, the FPZ might influence the relationship between the load and loading-line displacement. In this study, however, the crack propagation could not be observed at the onset of nonlinearity, but it occurred brittly when the load was close to its peak value. Therefore, the critical load for crack propagation P_c was provisionally determined to be the maximum load. In addition, the initial crack length was provisionally used for the analysis, although the determination method of effective crack length is described below. To determine the critical load and the effective crack length at the initiation of crack propagation in detail, however, further studies are required, especially because there are several definitions of the critical load for crack propagation [22].

By substituting P_c into Eq. (1), the nominal shear strength τ_{nc} corresponding to crack length $2a$ was obtained. Then the Mode II critical stress intensity factor K_{IIc} corresponding to the crack length was obtained by substituting $f(2a/s)$, which was determined by the finite element calculation and τ_{nc} in Eq. (2).

4.4. Three-point bend end-notched flexure tests

Mode II fracture mechanics properties can be determined precisely by end-notched flexure (ENF) test, which is of accordance to beam theory and energy considerations [15]. Therefore, it is meaningful to compare the K_{IIc} value obtained from the AFPB test with that obtained from the ENF test. Based on this concept, three-point bend end-notched flexure (3ENF) test was conducted and the results obtained were compared with those obtained from the AFPB tests.

Fig. 5 shows a diagram of 3ENF test. All of the specimens were cut from the lumber described above. The specimens with the TL-system had initial dimensions of 450 (L) × 30 (T) × 15 (R) mm^3.

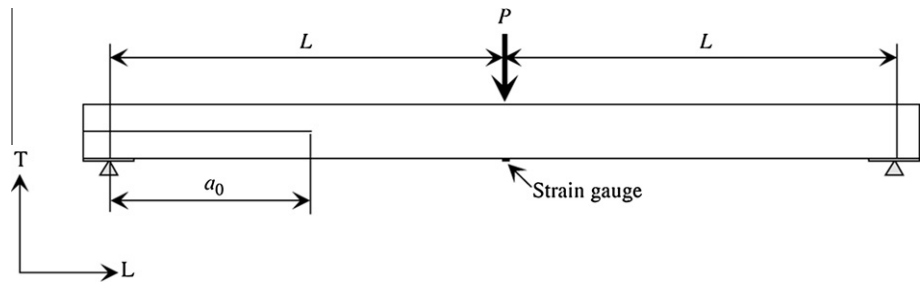

Fig. 5. Schematic diagram of the three-point bend end-notched flexure (3ENF) test. L, T, and R represent the longitudinal, tangential, and radial directions, respectively.

The crack was first cut with a band saw (thickness = 1 mm) then extended ahead of the crack tip with a razor blade. After the crack was cut in the specimen, two sheets of 0.5 mm-thick Teflon film were inserted between the crack surfaces to reduce the friction between the upper and lower cantilever beams. In the 3ENF test, the initial crack length a_0, which was defined as the distance from the support of the cracked portion to the crack tip, was 100 mm. The specimen was supported by 400-mm spans. As shown in Fig. 5, a steel platen 30 mm in length was placed between the specimen and the support to avoid an indentation at the supporting point. The platen could rotate around the supporting point. Therefore, it did not interrupt the deformation of the specimen. A load was applied to the midspan until the crack tip drew close to the midspan. The crosshead speed was 1 mm/min. The total testing time was about 10 min.

A displacement gauge was set below the midspan, and the loading-line displacement δ was obtained. The longitudinal strain ε_x was measured by a strain gauge (gauge length = 2 mm; FLA-2-11, Tokyo Sokki Kenkyujo Co., Ltd., Tokyo, Japan) that was bonded to the bottom surface of the midspan. The displacement gauge was set carefully in order not to touch the displacement rod on the strain gauge. The loading-line compliance C_L, the load at the onset of nonlinearity P_{NL}, and the load-longitudinal strain compliance C_S were determined. The Mode II initiation fracture toughness G_{IIc} was determined by substituting C_L, C_S, and P_{NL} into the following equation [6]:

$$G_{IIc} = \frac{3P^2 C_S}{4BLH}\left(2LH \cdot \frac{C_L}{C_S} - \frac{2}{3}L^3\right)^{\frac{2}{3}}, \tag{10}$$

where $2H$ is the depth of the specimen and B is the width of the beam and crack. The value of G_{IIc} was transformed into K_{IIc} by substituting E_x, E_y, G_{xy}, and n_{xy}, which correspond to E_L, E_T, G_{LT}, and n_{LT} in Table 1, respectively, into Eqs. (8) and (9). The values of K_{IIc} obtained by the 3ENF tests were compared with the values obtained by the AFPB tests.

5. Results and discussion

5.1. Finite element analyses

Fig. 6 shows the results of FE analyses. Fig. 6a shows the dependence of the loading-line compliance C on the half crack length a. The C–a relationship is regressed into the 4th polynomial function as follows:

$$C = 3.3496 \times 10^{-7} + 1.0087 \times 10^{-7}a + 2.9589 \times 10^{-5}a^2 + 2.2481 \times 10^{-3}a^3 - 1.124a^4. \tag{11}$$

Fig. 6b shows the normalised strain energy release rate G_{II}/P^2 calculated by the VCCT and compliance calibration method. Note that the values of G_{II}/P^2 obtained by the different methods are close to each other, so the C–a relationship shown in Fig. 6a is valid. Nevertheless, the value of C does not vary significantly with crack length, so the variation in C shown here would be obscured by measurement error in the actual AFPB test. This makes it difficult to obtain G_{IIc} by the compliance calibration method. In addition, the insensitivity of C on a makes it difficult to determine the effective crack length at the crack propagation, the detail of which is described below.

Fig. 7 shows the relationship between the crack geometry factor $f(2a/s)$ and the crack length-to-shear span ratio $2a/s$ obtained by finite element calculation. This relationship can be regressed into the following third polynomial equation:

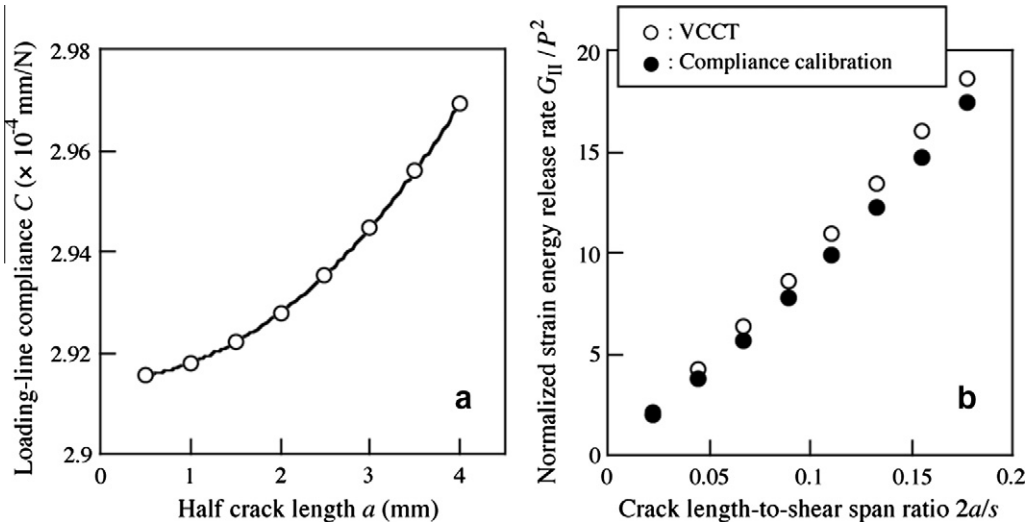

Fig. 6. Results of FE calculations of AFPB tests. (a) Dependence of the loading-line compliance C on the crack length a, and (b) comparison of the normalised strain energy release rates G_{II}/P^2 calculated by the virtual crack closure technique and compliance calibration method.

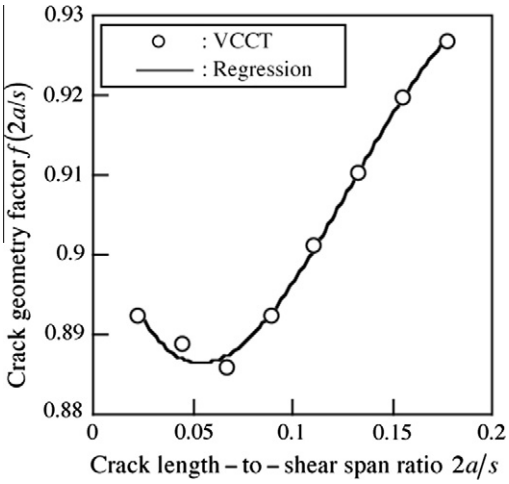

Fig. 7. Relationships between the crack geometry factor $f(2a/s)$ and the crack length-to-shear span ratio $2a/s$ obtained by the VCCT and the regressed equation represented as Eq. (12).

$$f\left(\frac{2a}{s}\right) = 0.90742 - 0.85428\left(\frac{2a}{s}\right) + 10.024\left(\frac{2a}{s}\right)^2 - 25.863\left(\frac{2a}{s}\right)^3. \tag{12}$$

The Mode II stress intensity factor was calculated using the crack geometry factor represented by Eq. (12).

5.2. Asymmetric four-point bending tests of cracked and crack-free specimens

Fig. 8 shows the relationship between the initial loading-line compliance C_0 and crack length $2a$ experimentally obtained and comparison with that obtained by the FE analyses. The C_0–$2a$ relationships coincide well with each other, so the relationship between the load and loading-line displacement can be obtained appropriately while reducing the influence of indentation. Nevertheless, the value of C_0 experimentally obtained varies significantly, so it is difficult to formulate the C–a relationship based on the experimental results, although it can be determined as Eq. (11) from the FEA results.

In Fig. 3, the failure of crack-free specimen ($2a = 0$ mm) is shown. As shown in this photograph, failure was induced along the neutral axis of the middle section for the crack-free specimen so that the value of τ_{nc} for the crack-free specimen could be regarded as the actual shear strength of the material.

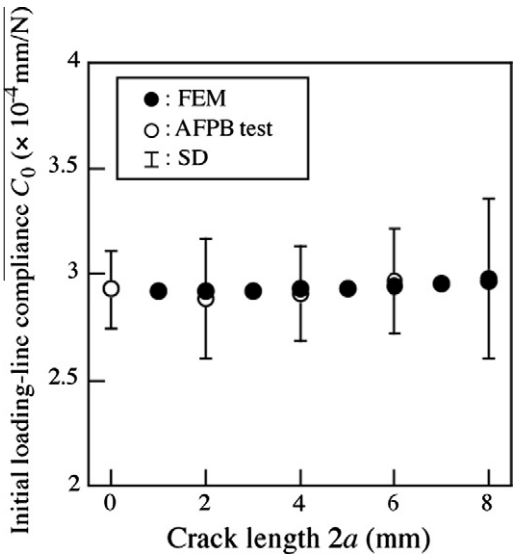

Fig. 8. Comparison of the loading-line compliances numerically and experimentally obtained.

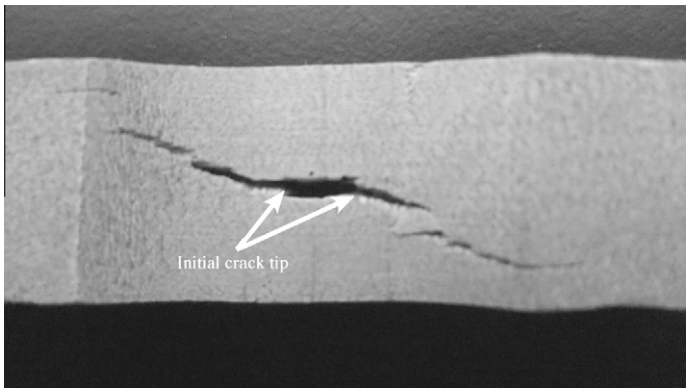

Fig. 9. Typical example of the crack path obtained in the asymmetric four-point bending specimen. Crack length $2a = 4$ mm.

Fig. 9 shows a typical example of the crack path in the AFPB specimen. The crack initially propagated straightforward by sliding, then it deviated from the neutral axis when the crack tip approached the loading line. There was a concern that mixed-mode loading condition was induced when the crack propagated obliquely. The indentation at the loading nose might influence on the curvature in the crack propagation because the crack tip approached to the loading line where the influence of indentation was marked. As shown in Fig. 9, however, the crack propagated straight at its initiation. Therefore, fracture mechanics theory could be applied for analysing the Mode II fracture behaviour.

Fig. 10 shows the relationship between the nominal shear strength τ_{nc} and the crack length $2a$. When conducting Thompson test, there were no outliers in the τ_{nc} values, so five specimens, which were used in one test condition, were also used to calculate the mean values and standard deviations. Statistical analysis revealed that the value of τ_{nc} was markedly smaller than that of the crack-free specimens. In the single-edge-notched bending (SENB) test of agathis, the nominal bending strength of a cracked specimen was markedly smaller than the strength of the crack-free specimen [3,4], so the tendency obtained here agrees with that obtained in the previous work [3,4]. This test result suggests that fracture mechanics theory is essential for analysing the failure behaviour of a cracked specimen even when the crack length is short.

Fig. 11 shows a comparison of K_{IIc}, obtained from the AFPB test, and K_{IIc}, from the 3ENF test. When conducting Thompson test, there were no outliers in the K_{IIc} values, so five specimens, which were used in one test condition, were also used to calculate the mean values and standard deviations. The value of K_{IIc} obtained using the peak load should be larger than those obtained using any other definitions of critical load. In this research, the critical load for crack propagation P_c was defined as the peak load in the AFPB test, so the K_{IIc} value obtained here was larger than those obtained under any other definitions of P_c. Nevertheless, statistical analysis revealed that K_{IIc} obtained from the AFPB test was significantly smaller than the value obtained from the 3ENF test at a significance level of 0.01. The analysis also revealed that the dependence of K_{IIc} on $2a$ was significant. Therefore, Eq. (2) could not be used for determining the appropriate K_{IIc} value.

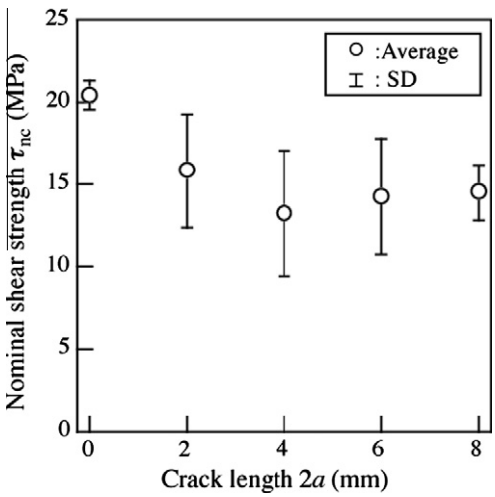

Fig. 10. Relationship between the nominal shear strength τ_{nc} and crack length $2a$.

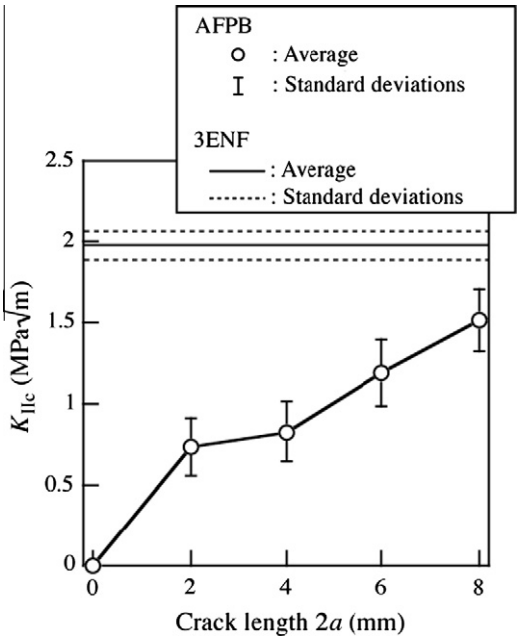

Fig. 11. Relationships between the Mode II critical stress intensity factor K_{IIc} and crack length $2a$ obtained by AFPB tests compared to the results obtained from 3ENF tests. K_{IIc} from the AFPB test was calculated using Eq. (2), in which the crack length was not corrected.

5.3. Consideration of additional crack length

According to previous studies, the cracked specimen often behaves as if the crack is longer than its actual length because of deformation around the crack tip, deflection caused by shearing force, and the development of an FPZ at the crack tip [3–8,19–30]. Therefore, it is feasible that the cracked AFPB specimens in this study also behaved as if the crack were longer than the actual length. The relationship between K_{II} and a can be moderated by introducing an additional crack length Δ into Eq. (2):

$$K_{II} = \tau_n \sqrt{\pi(a+\Delta)} f\left(\frac{2(a+\Delta)}{s}\right), \tag{13}$$

To determine the value of Δ, following two methods were examined: (1) compliance calibration method, and (2) comparison of the results obtained by the AFPB tests with those obtained by the 3ENF tests.

The equivalent crack length a_{eq}, in which the additional crack length is contained, is obtained from the relationship between loading-line compliance C and crack length a. When the C–a relationship is calibrated as $C = F(a)$ such as Eq. (11), the equivalent crack length a_{eq} can be determined using the loading-line compliance at the initiation of crack propagation (C_c in Fig. 4). The additional crack length Δ is then obtained as follows:

$$\Delta = a_{eq} - a_0, \tag{14}$$

where a_0 is the initial crack length. This method is valid from the viewpoint of energy considerations [7,8,15,19,21,23,25–27]. The value of a_{eq} was computed through a dichotomic process [25]. As described above, however, it was difficult to obtain the C–a relationship appropriately based on the experimental results. Although Eq. (11) was used instead of using the experimental results, the value of a_{eq} could not be obtained properly because the value of C_c varied in the same initial crack length a_0. To obtain the value of Δ by this method properly, the value of C should be sensitive to the variation of a. As described above, however, the insensitivity of C on a makes it difficult to determine the equivalent crack length at the crack propagation, although this method is valid.

Instead of using the relationship between the load and loading-line displacement, the value of Δ was obtained by comparing the data of 3ENF test. In the 3ENF test, the value of G_{IIc}, which can be determined with energy considerations and is mathematically well defined as described above [15]. Therefore, the value of K_{IIc} calculated by transforming the value of G_{IIc} obtained from the 3ENF test can be regarded as valid. In addition, the validity of ENF test has been variously verified in several previous investigations [5–10,12,32]. Although the comparison method is less rigorous mathematically than the compliance calibration method described above, it was effective for determining the Δ value, and this method was applied to the determination of Δ in the Mode I fracture system in the SENB, SENT, and CT tests of wood [29,30,33]. In a way similar to previous studies [29,30,33], the appropriate value of Δ was determined as follows: (1) By altering the value of Δ, the

P-value for the average values of K_{IIc} obtained by the AFPB test corresponding to each $2a$ and 3ENF test can be calculated; (2) The *P*-values corresponding to each Δ can be summed. When the amount of *P*-values is large, the average values of K_{IIc} obtained by the AFPB and 3ENF tests can be regarded as being close to one another. From this procedure, the additional crack length Δ is determined as 3.6 mm. In previous studies [20,26–28], the additional crack length was physically determined based on the concept of the FPZ, of which size depends on the specimen geometry, and the validity was verified by FEM analyses. This method may be effective for determining the value of Δ. From the test results, however, it was difficult to confirm that the value of Δ was based on FPZ production alone as described above. In addition, appropriate results were obtained when supposing a constant value of Δ for the specimens with a same geometry but with various crack length [29–32]. Therefore, the value of Δ was supposed to be constant, and the inverse method of the procedure described above was adopted. Further research should be carried out to determine the physical meaning of the additional crack length.

Fig. 12 shows the relationship between the Mode II critical stress intensity factor K_{IIc} and crack length $2a$. With the crack length correction, the dependence of K_{IIc} on the crack length was less significant than it was without the correction. Statistical analysis of the difference between the K_{IIc} values obtained using the AFPB and 3ENF tests showed that the difference was not significant, although testing conditions, such as the initial crack length, between the AFPB and 3ENF tests were extremely different from each other. Therefore, it was suggested that the crack-length correction was effective for analysing the Mode II fracture behaviour of wood, although the physical aspect of additional crack length was not sufficiently revealed.

Table 2 shows the average values of K_{IIc} obtained with and without crack-length correction. When the crack length was not corrected, the values shown in Table 2 were obtained by averaging the K_{IIc} values without using the data at $2a = 0$ mm, which is inevitably zero, although the value of K_{IIc} is dependent on crack length. In contrast, the dependence of K_{IIc} on the crack length was less significant when the crack length was corrected. As such, K_{IIc} was obtained by averaging all the data, including the data at $2a = 0$ mm. The relationships between τ_{nc} and a were predicted by substituting the values of K_{IIc}, a, and $f(2a/s)$ into Eq. (2), and K_{IIc}, a, Δ, and $f(2(a+\Delta)/s)$ into Eq. (13). Fig. 13 compares the predicted and experimentally obtained τ_{nc}–$2a$ relationships. When the crack length was not corrected, the predicted strength increased markedly as the crack length approached zero. When the crack length was corrected, however, the τ_{nc}–$2a$ relationship was effectively predicted over the full range of crack lengths, including $2a = 0$. Therefore, the failure-by-shearing behaviour, as well as the failure-by-bending behaviour, can be described by fracture mechanics theory even when the specimen has no crack [3,4].

As described above, it was difficult to reveal the source of the additional crack length Δ. Although the value of Δ obtained in this study may have been influenced by a FPZ, the value should be regarded as a correction of initial crack length. If the value of Δ was due to the FPZ alone, it can be physically determined and its validity can be verified by FEM analyses [23,26,27]. In addition, microscopic observations around the crack tip could be enhanced to reveal the source of Δ. It is required to evolve the testing method into that in which the loading-line compliance is sensitive to the variation of crack length even in the range of short length. Further studies, including appropriate loading conditions, FEM analyses,

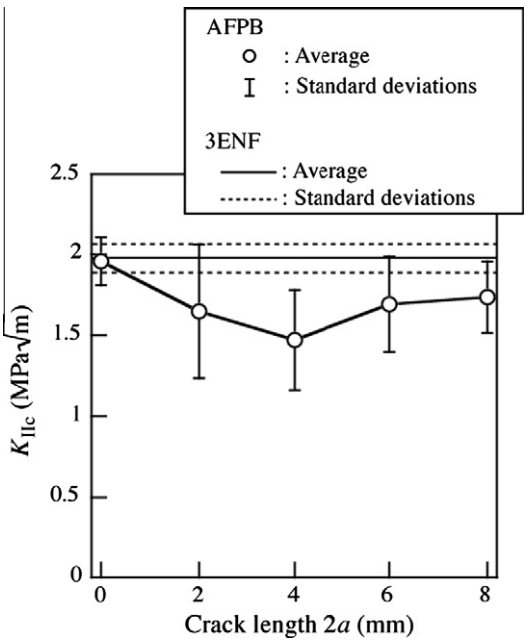

Fig. 12. Relationships between the Mode II critical stress intensity factor K_{IIc} and crack length $2a$ obtained by AFPB tests compared to the results obtained with 3ENF tests. K_{IIc} from the AFPB test was calculated using Eq. (13), in which the correction crack length Δ was taken into account.

Table 2
Mode II critical stress intensity factors K_{IIc} obtained with or without correcting the crack length.

Crack length uncorrected	Crack length corrected
1.10 ± 0.35[a]	1.73 ± 0.31[b]

The results are means ± SD.
[a] The crack lengths $2a$ used for obtaining K_{IIc} were 2, 4, 6 and 8 mm.
[b] The crack lengths $2a$ used for obtaining K_{IIc} were all data including those at $2a = 0$.

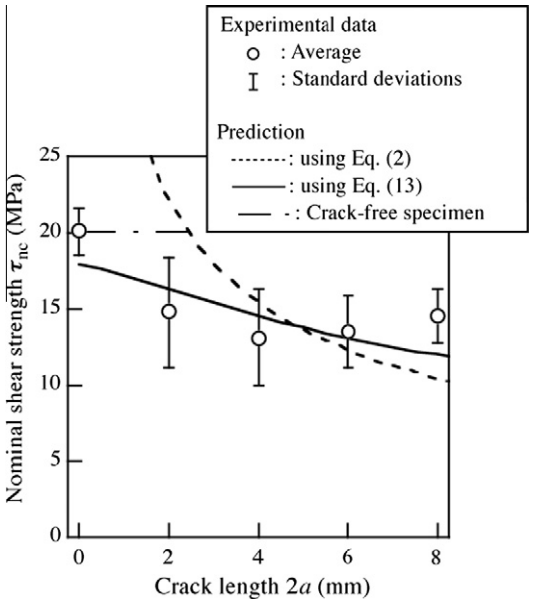

Fig. 13. Comparison of nominal shear strengths that were experimentally obtained or predicted on the basis of fracture mechanics theory.

microscopic observations, frequencies of the tests, and the improvement of testing method should be conducted to better understand this phenomenon.

6. Conclusion

Using agathis specimens, AFPB tests were conducted to analyse the failure behaviour of wood specimens containing a short crack under shear-dominant conditions. The results were compared to those obtained with 3ENF tests.

The nominal shear strength was markedly lower than the strength of a crack-free specimen. Therefore, the fracture mechanics theory was essential for analysing the failure behaviour of wood, even when the crack length was very short.

The Mode II critical stress intensity factor K_{IIc}, obtained with the AFPB test, decreased as the crack length approached zero. In addition, the K_{IIc} was significantly smaller than that obtained using the 3ENF test. With crack-length correction, however, the K_{IIc} obtained using the AFPB test was appropriately obtained over a wide range of crack lengths and was in agreement with the K_{IIc} obtained using the 3ENF test.

When the crack length was corrected, the relationship between the nominal shear strength and crack length was effectively predicted for the full range of crack lengths, even in a crack-free specimen.

Acknowledgements

The authors would like to thank Prof. Satoshi Sakamoto and Mr. He Wen of Shimane University for their help in conducting the experiment. This study was partly supported by a Grant-in-Aid for Scientific Research (C) (No. 21580207) of the Japan Society for the Promotion of Science (JSPS).

References

[1] Irwin GR, Kies JA, Smith HL. Fracture strength relative to onset and arrest of crack propagation. Proc ASTM 1958;58:640–57.
[2] Leicester RH. Application of linear fracture mechanics to notched timber elements. Prog Struct Engng Mater 2006;8:29–37.
[3] Susanti CME, Nakao T, Yoshihara H. Examination of the failure behaviour of wood with a short crack in the tangential–radial system by single-edge-notched bending test. Engng Fract Mech 2010;77:2527–36.

[4] Susanti CME. Study of failure behavior of wood with a short crack. PhD thesis, Shimane University, Japan; November 2010.
[5] Yoshihara H. Mode II *R*-curve of wood measured by 4-ENF test. Engng Fract Mech 2004;71:2065–77.
[6] Yoshihara H. Mode II initiation fracture toughness analysis for wood obtained by 3-ENF test. Compos Sci Technol 2005;65:2198–207.
[7] Silva MAL, de Moura MFSF, Morais JJL. Numerical analysis of the ENF test for mode II wood fracture. Composites A 2006;37:1334–44.
[8] de Moura MFSF, Silva MAL, de Morais AB, Morais JJL. Equivalent crack based mode II fracture characterization of wood. Engng Fract Mech 2006;73:978–93.
[9] Arrese A, Carbajal N, Vegas G, Mujika F. A new method for determining mode II *R*-curve by the End-Notched Flexure test. Engng Fract Mech 2010;77:51–70.
[10] Valentin G, Caumes P. Crack propagation in mixed mode in wood: a new specimen. Wood Sci Technol 1989;23:43–53.
[11] Stanzl-Tschegg SE, Tan DM, Tschegg EK. Mode II fracture tests on spruce wood. Mokuzai Gakkaishi 1996;42:642–50.
[12] Murphy JF. Mode II wood test specimen: beam with center slit. J Test Eval 1988;16:364–8.
[13] Yoshihara H, Furushima T. Shear strengths of wood measured by various short beam shear test methods. Wood Sci Technol 2003;37:189–97.
[14] Yoshihara H, Suzuki A. Shear stress/shear strain relation of wood obtained by asymmetric four-point bending test of side-tapered specimen. J Test Eval 2005;33:55–60.
[15] Adams DF, Carlsson LA, Pipes RB. Experimental characterization of advanced composites materials. 3rd ed. Boca Raton: CRC Press; 2003.
[16] Zhao D, Wang Y. Mode III fracture behavior of laminated composite with edge crack in torsion. Theor Appl Fract Mech 1998;29:109–23.
[17] Sih GC, Paris PC, Irwin GR. On cracks in rectilinearly anisotropic bodies. Int J Fract Mech 1965;1:189–203.
[18] Hearmon RFS. The influence of shear and rotatory inertia on the free flexural vibration of wooden beams. Brit J Appl Phys 1958;9:381–8.
[19] Morel S, Bouchaud E, Schmittbuhl J. Influence of the specimen geometry on *R*-curve behavior and roughening of fracture surfaces. Int J Fract 2003;121:23–42.
[20] Bažant ZP. Concrete fracture model: testing and practice. Engng Fract Mech 2002;69:165–205.
[21] Dourado N, Morel S, de Moura MFSF, Valentin G, Morais J. Comparison of fracture properties of two wood species through cohesive crack simulations. Composites A 2008;39:415–27.
[22] Davies P, Blackman BRK, Brunner AJ. Mode I delamination. In: Moore DR, Pavan A, Williams JG, editors. Fracture mechanics testing methods for polymers adhesives and composites. ESIS Publication 28. Amsterdam: Elsevier; 2001.
[23] de Moura MFSF, Dourado N, Morais JJL. Crack equivalent based method applied to wood fracture characterization using the single edge notched-three point bending test. Engng Fract Mech 2010;77:510–20.
[24] Williams JG, Hadavinia H. Analytical solutions for cohesive zone models. J Mech Phys Solids 2002;50:809–25.
[25] Morel S, Dourado N, Valentin G, Morais J. Wood: a quasibrittle material *R*-curve behavior and peak load evaluation. Int J Fract 2005;131:385–400.
[26] de Moura MFSF, Morais JJL, Dourado N. A new data reduction scheme for mode I wood fracture characterization using the DCB test. Engng Fract Mech 2008;75:3852–65.
[27] de Moura MFSF, Campilho RDSG, Gonçalves JPM. Crack equivalent concept applied to the fracture characterization of bonded joints under pure mode I loading. Compos Sci Technol 2008;68:2224–30.
[28] Zhao Z, Kwon SH, Shah SP. Effect of specimen size on fracture energy and softening curve of concrete: Part I. Experiments and fracture energy. Cem Concr Res 2008;38:1049–60.
[29] Yoshihara H. Examination of the mode I critical stress intensity factor of wood obtained by single-edge-notched bending test. Holzforscung 2010;64:501–9.
[30] Yoshihara H. Influence of loading condition on the measurement of mode I critical stress intensity factor of wood and medium density fiberboard by the single-edge-notched tension test. Holzforschung 2010;64:735–45.
[31] Yoshihara H, Kawamura T. Mode I fracture toughness estimation of wood by DCB test. Composites A 2006;37:2105–13.
[32] Yoshihara H. Influence of crack length on the measurement of mode II initiation fracture toughness of wood by three-point bend end-notched flexure (3ENF) test. Trans J Soc Mech Eng 2006;72:133–9.
[33] Yoshihara H, Usuki A. Mode I critical stress intensity factor of wood and medium-density fiberboard measured by compact tension test. Holzforschung 2011;65:729–35.